Regions of Attraction for Hybrid Limit Cycles of Walking Robots

Ian R. Manchester, Mark M. Tobenkin, Michael Levashov, Russ Tedrake

CSAIL, Massachusetts Institute of Technology, USA.

{irm, mmt, levashov, russt}@mit.edu

Abstract—This paper illustrates the application of recent research in region-of-attraction analysis for nonlinear hybrid limit cycles. Three example systems are analyzed in detail: the van der Pol oscillator, the "rimless wheel", and the "compass gait", the latter two being simplified models of underactuated walking robots. The method used involves decomposition of the dynamics about the target cycle into tangential and transverse components, and a search for a Lyapunov function in the transverse dynamics using sum-of-squares analysis (semidefinite programming). Each example illuminates different aspects of the procedure, including optimization of transversal surfaces, the handling of impact maps, optimization of the Lyapunov function, and orbitally-stabilizing control design.

I. Introduction

The purpose of this paper is to illustrate a new technique for estimation of regions of attraction for nonlinear hybrid limit cycles proposed in [1]. Three example systems have been chosen which illuminate different aspects of the method.

A major motivation for the work in this paper is control of underactuated "dynamic walking" robots ([2]). These robots can exhibit efficient, naturalistic, and highly dynamic gaits. However, control design and stability analysis for such robots is a challenging task since their dynamics are intrinsically hybrid and highly nonlinear.

Estimates of regions of attraction can be useful for many problems, including analysis of different candidate control laws, generation of tree-based feedback motion-planning controllers ([3]), or planning transitions among a library of pre-stabilized walking gaits ([4]).

The method involves choosing a decomposition of the dynamics into tangential and transversal components, and then searching for a Lyapunov function in the transversal components that verifies a "tube" about the limit cycle in which orbital stability is guaranteed. The verification is performed using sum-of-squares (SoS) programming.

The first example is the van der Pol oscillator, chosen because it is very well-known and well studied, and thus provides a good test of the method. With this example, we illustrate the importance of selecting the transversal decomposition intelligently. Indeed, it is shown that the commonly-used orthogonal transversal surfaces are often a bad choice.

The second is the "rimless wheel", a one-degree-of-freedom hybrid mechanical system, which serves as a simple model of a walking robot. The dynamics of the sytem are simple enough

that much can be said about the rimless wheel analytically. Despite being simple, it exhibits hybrid (switching) behaviour representing the foot fall of a walking robot.

The third example is the "compass-gait" walker, a more complex model of a walking robot. For this system, one cannot derive analytical regions of attraction, so a computational approach is essential. This system requires transversal surface optimization, proper handling of impacts, and also orbitally-stabilizing control design based on a transverse linearization.

A. Background

The most well-known tool for analysing limit cycles is the Poincaré map: orbital stability is characterized by stability of an associated "first-return map", describing the repeated passes of the system through a single transversal hypersurface. Often a linearization of the first-return map is computed numerically, and its eigenvalues can be used to verify local orbital stability. Since the system's evolution is only analyzed on a single surface, regions of stability in the full state-space are difficult to evaluate via the Poincaré map.

A related technique known variably as "transverse coordinates" or "moving Poincaré sections" also has a long history and was certainly known to exist by Poincaré, however has not been much used in applications until recently due to difficulty in the relevant computations (see [5]). With this technique, a new coordinate system is defined on a family of transversal hypersurfaces which move about the orbit under study. In most cases, it is also used to study local stability, however it can be adapted to characterize regions of stability in the full state space.

The method we propose is to construct the transverse dynamics in regions of the orbit, and then utilize the well-known sum-of-squares (SoS) relaxation of polynomial positivity which is amenable to efficient computation via semidefinite programming (see, e.g., [6], [7], [8]). The sum-of-squares relaxation has been previously used to characterize regions of stability of equilibria of nonlinear systems (see, e.g., [9], [10], [11]) and as a tool for constructive control design in [3].

There is comparatively little work on computing regions of stability of limit cycles. The proposed method has aspects in common with the surface Lyapunov functions proposed in [12], however that method was restricted to piecewise linear systems. The technique of cell-to-cell mapping, proposed by [13], improves the efficiency of exhaustive grid-based methods of regional analysis and has been used in analysis of simple

walking robots ([14]), however the computational cost is still exponential in the dimension of the system.

II. PROBLEM STATEMENT

We consider the following class of hybrid systems with planar switching surfaces:

$$\dot{x} = f(x, u), \ x \notin S^- \qquad (1)$$
$$x^+ = \Delta(x), \ x \in S^-. \qquad (2)$$

where $x \in \mathbb{R}^n$, and $u \in \mathbb{R}^m$. Suppose $f(\cdot)$ and $\Delta(\cdot)$ are smooth and $\Delta : S^- \to S^+$ where

$$S^- = \{x : c'_- x = d_-\}, \qquad (3)$$
$$S^+ = \{x : c'_+ x = d_+\}, \qquad (4)$$

$c_-, c_+ \in \mathbb{R}^n$, and $d_-, d_+ \in \mathbb{R}$. Suppose $x^\star(\cdot)$ is a non-trivial T-periodic solution that undergoes N impacts at times $\{t_1, t_2, ..., t_N\} + kT$ for integer k. We will assume that the impacts are not "grazing", i.e. $c'_- f(x^\star(t_i)) \neq 0$ and $c'_+ f(x^\star(t_i)) \neq 0$ for all i.

It is well-known that periodic solutions of autonomous systems cannot be asymptotically stable, since perturbations in phase are persistent. The more appropriate notion is *orbital stability* (see, e.g., [5], [15], [16]).

The analysis objective is to efficiently compute a region of state space $D \subset \mathbb{R}^n$ from which orbital stability to $x^\star(\cdot)$ is guaranteed.

III. TRANSVERSE DYNAMICS AND REGIONS OF ORBITAL STABILITY

In this section we briefly describe the process of verifying regions of orbital stability. Full details of each step are given in [1].

The process we propose for finding regions of orbital stability is based on the construction of a smooth local change of coordinates $x \to (x_\perp, \tau)$. At each point $t \in [0, T]$ we define a hyperplane $S(t)$, with $S(0) = S(T)$, which is transversal to the solution $x^\star(\cdot)$, i.e. $\dot{x}^\star(t) \notin S(t)$.

The transversal surfaces are defined by:

$$S(\tau) = \{y \in \mathbb{R}^n : z(\tau)'(y - x^\star(\tau)) = 0\}$$

where $z : [0, T] \to \mathbb{R}^n$ is a vector function which will be optimized.

Given a point x nearby $x^\star(\cdot)$, the scalar $\tau \in [0, T)$ represents which of these transversal surfaces $S(\tau)$ the current state x inhabits; the vector $x_\perp \in \mathbb{R}^{n-1}$ is the "transversal" state representing the location of x within the hyperplane $S(\tau)$, with $x_\perp = 0$ implying that $x = x^\star(\tau)$. This is visualised in Figure 1.

The process for computing regions of orbital stability is as follows:

1) Select a family of transversal surfaces $S(\tau)$, and the associated transformation $x \to (x_\perp, \tau)$ such that at impact times the transversal surfaces line up with switching surfaces.
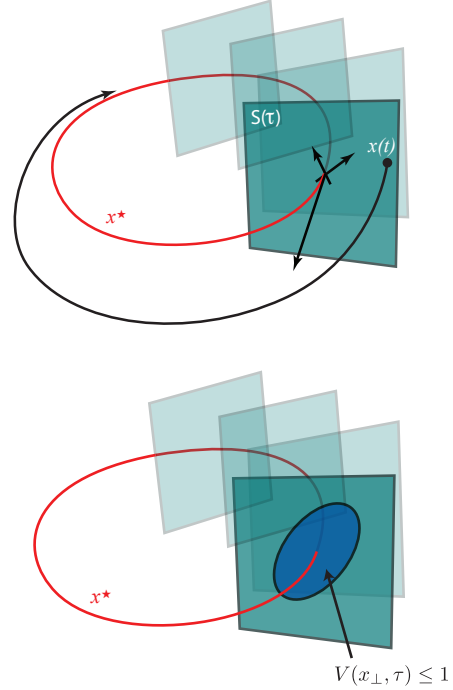2) Compute the nonlinear dynamics in this new coordinate system as well as a periodic linear system representing the dynamics of $x_\perp$ close to the orbit: the *transverse linearization*.
3) Construct a candidate quadratic Lyapunov function associated with the transverse linearization via standard techniques from linear control theory.
4) Using this result as an initial seed, iteratively solve a sequence of sum-of-squares programs to compute maximal regions in which a Lyapunov function can be found verifying both well-posedness of the change of coordinates and orbital stability for the true nonlinear dynamics.

Fig. 1. Top: transversal surfaces $S(\tau)$ around the target orbit $x^\star$, with a particular solution $x(t)$ converging to the orbit $x^\star$. Bottom: a Lyapunov function defined on a transversal surface.

For each $\tau \in [0, T]$, $\Pi(\tau) \in \mathbb{R}^{(n-1) \times n}$ is a smooth matrix function of τ projecting $x \to x_\perp$.

The dynamics in the new coordinates $x_\perp, \tau$ are given by the continuous dynamics

$$\dot{x}_\perp = \dot{\tau} \left[\frac{d}{d\tau} \Pi(\tau) \right] \Pi(\tau)' x_\perp + \Pi(\tau) f(x^\star(\tau) + \Pi(\tau)' x_\perp)$$
$$- \Pi(\tau) f(x^\star(\tau)) \dot{\tau}, \qquad (5)$$
$$\dot{\tau} = \frac{z(\tau)' f(x^\star(\tau) + \Pi(\tau)' x_\perp)}{z(\tau)' f(x^\star(\tau)) - \frac{dz(\tau)}{d\tau}' \Pi(\tau)' x_\perp}, \qquad (6)$$

for $t \neq t_i$, and impact updates

$$x_\perp^+ = \Pi(\tau_i^+) \left[\Delta_i \big(x^\star(\tau_i^-) + \Pi(\tau_i^-)' x_\perp^- \big) - x^\star(\tau_i^+) \right], \quad (7)$$

when $t = t_i$. The change of coordinates and the above dynamics are well-defined in a region around the target orbit $x^\star(\cdot)$.

A. Regions of Orbital Stability

Suppose there exists a Lyapunov function V such that $V(x_\perp, \tau) > 0, x_\perp \neq 0, V(0, \tau) = 0$ for all $\tau \in [0, T]$ for which the following conditions hold on the level set $\{x : V(x_\perp, \tau) \leq 1\}$:

$$\frac{d}{dt} V(x_\perp, \tau) \leq -\delta |x_\perp|^2, \quad (8)$$

$$z(\tau)' f(x^\star(\tau)) - \frac{\partial z(\tau)'}{\partial \tau} \Pi(\tau)' x_\perp > 0, \quad (9)$$

for some $\delta > 0$. The first constraint verifies stability via the decreasing Lyapunov function; the second verifies well-posedness of the change of variables. If hybrid dynamics are considered, at the switching times one must verify the condition:

$$V\left(\Pi(\tau_i^+)\left[\Delta_i\left(x^\star(\tau_i^-) + \Pi(\tau_i^-)'x_\perp\right)\right.\right.$$
$$\left.\left. -x^\star(\tau_i^+)\right], \tau_i^+\right) - V(x_\perp, \tau_i^-) \leq 0, \quad (10)$$

If these conditions hold then the set $\{x : V(x_\perp, \tau) \leq 1\}$ is an inner (conservative) estimate of the region of attraction to the limit cycle. Furthermore, for polynomial dynamics these can be relaxed to a SoS program. In some cases, one must also check that the impact surface is not reached before it is expected (see [1]).

Typically we sample a sufficiently fine finite sequence of $\tau \in [0, T]$ and verify the conditions on $x_\perp$ at each sample. In the optimization procedure, one must search for both $V(x_\perp, \tau)$ and Lagrange multipliers verifying the regional conditions. This problem is non-convex, however when fixing $V(x_\perp, \tau)$ and searching over Lagrange multipliers it is a semidefinite program, and when fixing Lagrange multipliers and searching over $V(x_\perp, \tau)$ it is a semidefinite program. Thus if one has a reasonable initial guess for $V(x_\perp, \tau)$ an iterative procedure can be applied. Whilst this is not guaranteed to find a global optimum, in practice the authors have found it works very well.

B. Transverse Linearization

In the construction of initial candidate Lyapunov functions and feedback controllers, we will make use of the linearization of the transverse dynamics:

$$\dot{x}_\perp = A(t)x_\perp(t) + B(t)\bar{u}(t), \quad t \neq t_i \quad (11)$$
$$x_\perp^+ = A_d x_\perp, \quad t = t_i. \quad (12)$$

representing the parts of (5) and (7) linear in $x_\perp$. Note that this can be given analytically for any system in the class.

IV. THE VAN DER POL OSCILLATOR

The first example we consider is the van der Pol oscillator, defined by the following differential equation:

$$\ddot{y} - \mu(1 - y^2)\dot{y} + y = 0.$$

where μ is a constant, which we take equal to 1. It is well-known that this system has a single unstable equilibrium at the origin, and a periodic cycle which is the limit from every
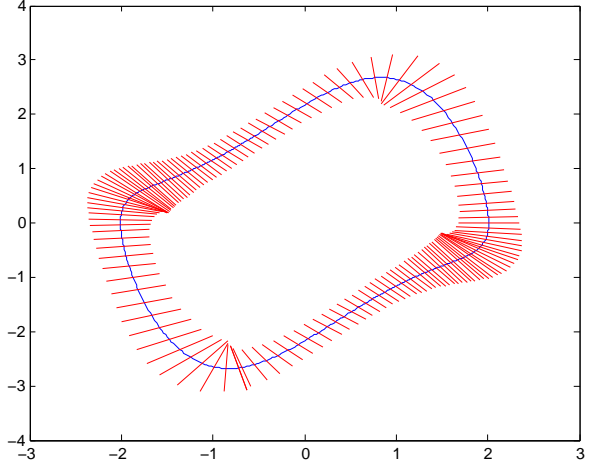

Fig. 2. Verified regions of orbital stability using constant rescalings of linear Lyapunov function and orthogonal transversal surfaces.

other point in the plane. Thus, it makes a good simple example on which to test the proposed method. The above differential equation can obviously be rewritten in terms of a state $x = [x_1 \ x_2]' := [y \ \dot{y}]'$ in the form

$$\dot{x} = f(x), \ f(x) = \begin{bmatrix} x_2 \\ (1 - x_1^2)x_2 - x_1 \end{bmatrix}.$$

To compute the periodic solution $x^\star$ we simply simulated the system forward from an initial condition away from the origin until it converged. Let T be its period.

Given a vector $z(\tau)$, for a planar system the projection $\Pi(\tau)$ onto surfaces orthogonal to $z(\tau)$ is simple: $\Pi(\tau) = [-z_2(\tau) \ z_1(\tau)]$. We start with transversal surfaces orthogonal to the system motion, i.e. $z(\tau) = f(x^\star(\tau))/|f(x^\star(\tau))|$.

A natural candidate for a Lyapunov function is the solution of the Lyapunov differential equation for the transverse linearization:

$$\dot{P}(t) + A(t)'P(t) + P(t)A(t) + Q = 0. \quad (13)$$

For any $Q > 0$ a unique periodic solution $P(t) = P(t + T) > 0$ exists, and suggests a Lyapunov function of $x_\perp P(\tau)x_\perp$, as was suggested in [15].

We can then search for the maximal level set $x_\perp P(\tau)x_\perp \leq \rho$ in which stability can be verified. In the framework of Section III-A this corresponds to verifying (8) and (9) for Lyapunov fuction of the form $V(x) = (1/\rho)x_\perp P(\tau)x_\perp$, which can be performed via a simple bisection search over ρ. The results are shown in Figure 2.

The regions are strongly limited by points at which the change of variables $x \to (x_\perp, \tau)$ becomes ill-defined. In the figure, these points resemble the hub of a bicycle wheel. Mathematically, they correspond to points at which the denominator of (6) goes to zero. This is clearly a consequence of the choice of transversal surfaces and motivates exploring other possible choices.

The van der Pol oscillator is a special case, since we know in advance that an orbital stability test must fail at the origin, the unstable equilibrium. With this in mind we construct radial transversal surfaces centred at the origin. Since $z(\tau)$ and $\Pi(\tau)$
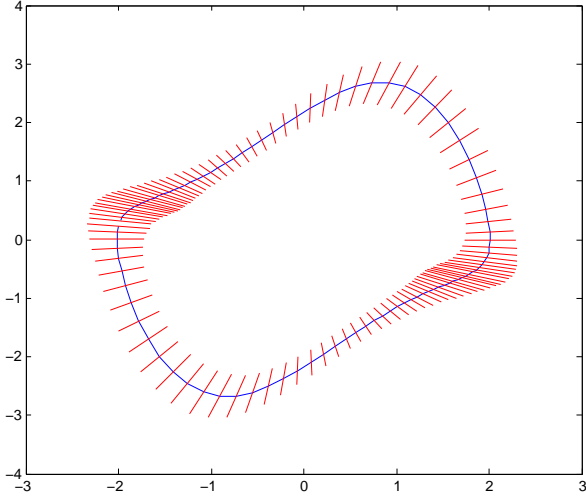
Fig. 3.   Verified regions of orbital stability using constant rescalings of linear Lyapunov function and radial transversal surfaces.
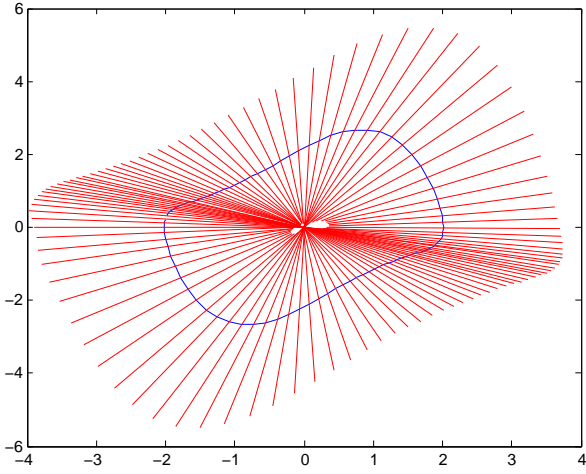

Fig. 5.   The function $\sigma(\tau)$ used to verify the region in Fig 4.

Fig. 4.   Verified regions of orbital stability using time-varying $\sigma(\tau)$ and radial transversal surfaces.

Fig. 6.   Verified regions of orbital stability using time-varying $\sigma(\tau)$ and locally-optimized transversal surfaces.

are changed, we recompute the solution of (13) and again search for the maximal level set of this Lyapunov function.

The results are plotted in Figure 3. We no longer have the problem with singularities, however the regions are still quite thin. The reason is that whilst the Lyapunov ODE is guaranteed to *locally* verify orbital stability (see [15]), it may not be a very good choice for verifying *regional stability*.

The result is much improved if we allow time-varying adjustment to the Lyapunov function via a scaling function $\sigma(\tau) > 0$, i.e.

$$V(x_\perp, \tau) = \sigma(\tau) x_\perp' P(\tau) x_\perp \qquad (14)$$

where $\sigma(\cdot) : [0, T] \to \mathbb{R}$, $\sigma(0) = \sigma(T)$, and $P(\tau)$ is as above.

The results are plotted in Figure 4. This figure is computed with $\sigma(\tau)$ a Bezier polynomial of order 20. It is observed that increasing the order of $\sigma(\tau)$ grows the region essentially to the origin.

Note that since we are searching over a class of candidate Lyapunov functions which are symmetric with respect to the
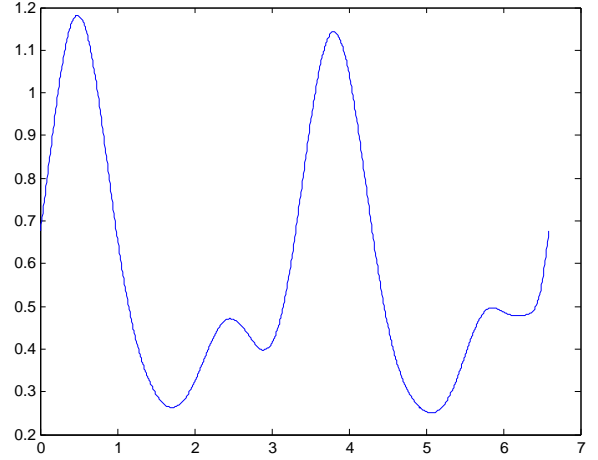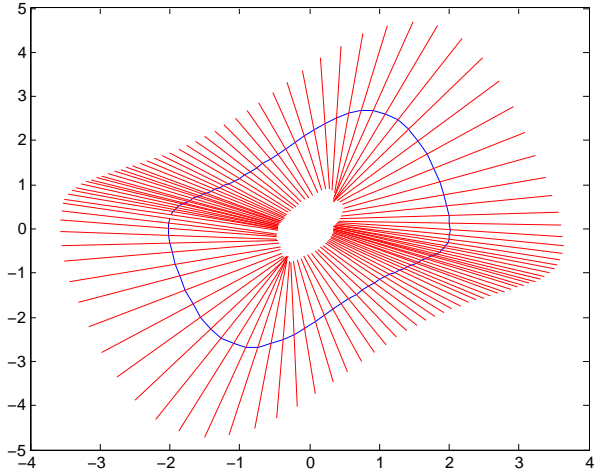
orbit, the computed region is the best that can be achieved. The time-varying rescaling that achieved this is shown in Figure 5.

To obtain these results we made use of qualitative knowledge of the true region of stability in order to choose the transversal surfaces, which will not be possible for more complicated systems. In [1] a procedure for choosing $z(\tau)$ was suggested which depends only on local information about $f(x^\star, u^\star)$. The idea is to optimize the function $z(\tau)$ so that the distance to the closest point of singularity is maximized. The results of applying this procedure are shown in Figure 6.

This choice of transversal surfaces does not do quite as well the radial surfaces, which is not surprising. However it does substantially better than the orthogonal surfaces in Fig. 2. It seems there is still plenty of room for improvement in the optimization of $z(\tau)$, perhaps in an iterative procedure based on results of a prior region-of-stability computations.

V. RIMLESS WHEEL

The rimless wheel is a simple planar model of walking and consists of a central mass with several 'spokes' extending

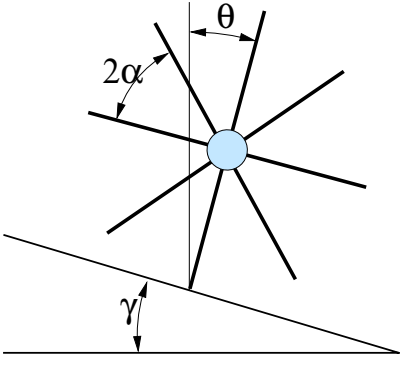Fig. 7.   Rimless wheel system

Fig. 8.   Phase portrait of the rimless wheel system.

radially outward. (See Figure 7). At any given moment one of the spokes is pinned at the ground, and the system follows the dynamics of a simple pendulum, $f(\theta, \dot\theta) = [\dot\theta, \sin(\theta)]'$. When another spoke contacts the ground, the system undergoes an inelastic collision governed by $\dot\theta^+ = \cos(2\alpha)\dot\theta$, and the new spoke becomes the pinned one.

On a sufficiently inclined slope the system has a stable limit cycle, for which the energy lost in collision is perfectly compensated by the change in potential energy. The rimless wheel has been analyzed in the literature and the basin of attraction has been computed exactly (see [17]). It is interesting to see how close our region of attraction estimation method can approximate the actual basin for this system.

Figure 8 shows the phase portrait of the rimless wheel, with arrows indicating the direction of the dynamics. The right edge of the graph represents the collision surface that maps to the left edge of the graph (or vice-versa, depending on the direction of dynamics). Because the impact depends only on the value of the angle, θ, and not on $\dot\theta$, the collision surfaces are vertical. The thick green lines are the homoclinic orbits of the simple pendulum. The thick black line shows the stable limit cycle, and the shading shows a subset of its true region of attraction.

In this case, it is natural to select vertical transversal surfaces, since there are no singularities in the change of variables, and the transversal surfaces are aligned with switching surfaces. The surfaces can be parametrized by θ as $\tau = \tau(\theta)$, and the nominal trajectory is simply $\theta^\star(\theta) = \theta$ and $\dot\theta^\star(\theta) = \sqrt{2E - 2\cos(\theta)}$, where E is the total energy of the system. Then the transversal coordinate is the vertical position with respect to the nominal trajectory: $x_\perp = \dot\theta - \dot\theta^\star(\theta)$.

With this choice of transversal surfaces, the dynamics in the new coordinate system are straightforward to compute:

$$\dot x_\perp = \ddot\theta - \frac{d}{dt}\dot\theta^\star(\theta) = \sin(\theta) - \frac{d\dot\theta^\star}{d\theta}(\theta)\dot\theta$$
$$= \sin(\theta) - \frac{\sin(\theta)}{\dot\theta^\star(\theta)}\dot\theta = -\frac{\sin(\theta)}{\dot\theta^\star(\theta)}x_\perp. \quad (15)$$

Interestingly, the transversal dynamics are linear for any given θ. Note that the transverse dynamics are also easily derived from equations (5) and (6) by setting $z(\tau) = [1, 0]'$ and $\Pi(\tau) = [0, 1]$. This gives $\dot\tau = \frac{\dot\theta}{\dot\theta^\star(\theta)}$ and the equation (15), as expected.
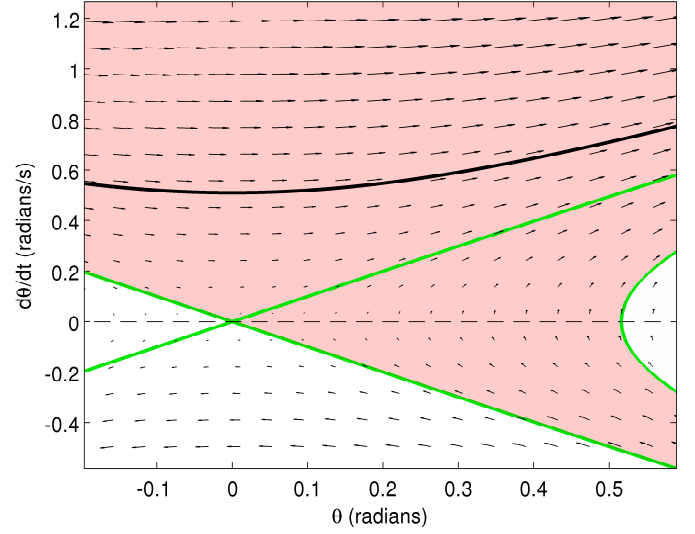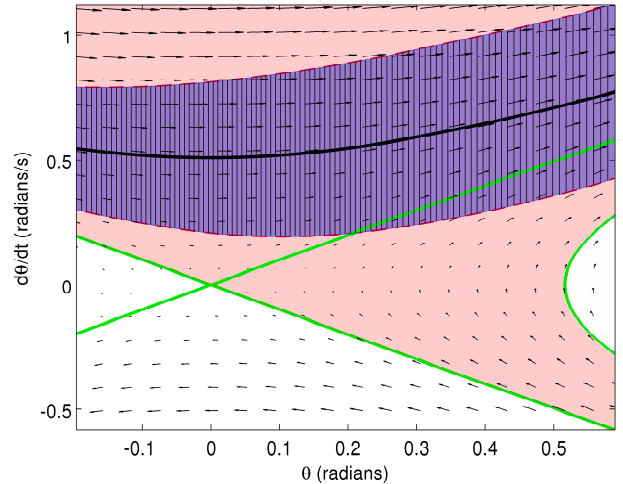

Fig. 9.   Regions of Attraction for the rimless wheel limit cycle. Light shaded region is the true RoA. Dark shaded region is the verified RoA.

As with the van der Pol oscillator, to find an initial candidate Lyapunov function we computed the unique periodic solution of the jump Lyapunov differential equation:

$$-\dot P(t) = A(t)'P(t) + P(t)A(t) + Q, \ t \neq t_i$$
$$P(\tau_i^-) = A_d(\tau_i)'P(\tau_i^+)A_d(\tau_i) + Q_i, \ t = t_i$$

with $Q, Q_i > 0$ and search over scalar rescalings: $V(x) = (1/\rho)x_\perp' P(\tau)x_\perp$.

Figure 9 shows the results. The discrete set of transverse surfaces can be seen as thin black vertical lines around the orbit. The computed basin of attraction (dark shading) is within the true basin (light shading), but doesn't fill it fully. This is not surprising, since we searched over a very restrictive set of Lyapunov functions.
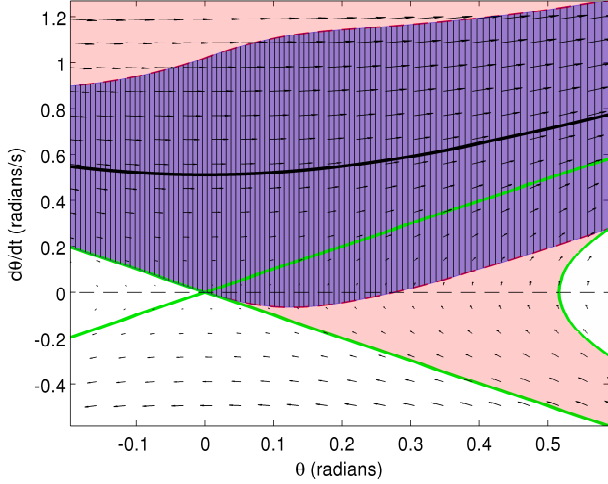
Fig. 10. Regions of Attraction for the rimless wheel limit cycle. Light shaded region is the true RoA. Dark shaded region is the verified RoA.
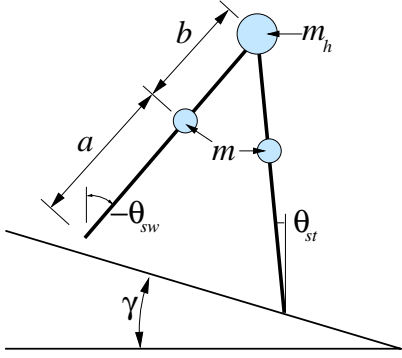

Fig. 11. Compass gait system

We then searched over 10th-order rescaling polynomials $\sigma(\tau)$, as in (14), to maximize area of the computed region. Figure 10 shows the results and, as expected, the basin of attraction is larger.

Note that the verified basin of attraction includes regions where $\dot{\theta} < 0$ and, by the choice of transverse surfaces, $\dot{\tau} < 0$. The verification procedure still holds when the system state moves backwards through the transverse surfaces.

VI. COMPASS-GAIT WALKER

The compass-gait walker is a two-degree-of-freedom (four-state) nonlinear hybrid system shown in Figure 11. Similarly to the rimless wheel, one of the legs (the "stance leg") is always pinned at the ground, and the other (the "swing leg") swings until it hits the ground, at which point the swing leg becomes the stance leg and vice versa. A motor at the hip generates torque, τ, between the legs. Letting $q = [\theta_{sw}, \theta_{st}]'$, $u = \tau$, and $l = a + b$ the continuous dynamics can be expressed in the standard manipulator form as

$$H(q)\ddot{q} + C(q, \dot{q})\dot{q} + G(q) = Bu,$$

where

$$H = \begin{bmatrix} mb^2 & -mlb\cos(\theta_{st} - \theta_{sw}) \\ -mlb\cos(\theta_{st} - \theta_{sw}) & (m_h + m)l^2 + ma^2 \end{bmatrix},$$

$$C = \begin{bmatrix} 0 & mlb\sin(\theta_{st} - \theta_{sw})\dot{\theta}_{st} \\ -mlb\sin(\theta_{st} - \theta_{sw})\dot{\theta}_{sw} & 0 \end{bmatrix},$$

$$G = \begin{bmatrix} mbg\sin(\theta_{sw}) \\ -(m_h l + ma + ml)g\sin(\theta_{st}) \end{bmatrix}, B = \begin{bmatrix} 1 \\ -1 \end{bmatrix}.$$

At the moments of impact, the coordinates undergo a relabling: $\theta_{sw}^+ = \theta_{st}$ and $\theta_{st}^+ = \theta_{sw}$. The impact dynamics for velocities are derived assuming a perfect inelastic collision:

$$Q_\alpha^+ \dot{q}^+ = Q_\alpha^- \dot{q}^-$$

where

$$Q_\alpha^- = \begin{bmatrix} -mab & -mab + (m_h l^2 + 2mal)\cos(2\alpha) \\ 0 & -mab \end{bmatrix}$$

$$Q_\alpha^+ = \begin{bmatrix} mb(b - l\cos(2\alpha)) & ml(l - b\cos(2\alpha)) + ma^2 + m_h l^2 \\ mb^2 & -mbl\cos(2\alpha) \end{bmatrix}$$

and $\alpha = \frac{\theta_{sw} - \theta_{st}}{2}$. The impact takes place when $\theta_{sw} + \theta_{st} + 2\gamma = 0$, where γ is the slope of the ground. Note that although the switching dynamics are highly nonlinear, the switching *surfaces* are planar, matching the assumptions of [1].

For some combination of parameters and initial conditions the system exhibits a limit cycle behavior of walking downhill passively (with zero torque). For this reason, the model is often used for studying bipedal walking (see, e.g. [18], [19], [20], [21], [22] and many others). Prior to this work, studies of the small basin of attraction of this system were limited to exhaustive simulation.

We orbitally stabilize the limit-cycle using LQR control in the transverse coordinates, and analyze the region of attraction for the closed loop system. We begin by computing the T-periodic stable limit cycle solution numerically from suitable initial conditions. We next optimize for a set of transversal surfaces at $N = 40$ sample points along the trajectory. These surfaces are constrained to align with planar switching surfaces capturing the "swing leg" losing then regaining contact with the ground. We construct the transverse coordinates, and the resulting transverse dynamics.

A set of transversal surfaces were chosen via the optimization procedure suggested in [1]. An LQR controller was then designed for the transverse linearization by solving for the periodic positive-definite solution of the jump-Riccati equation:

$$-\dot{P} = A'P + SA - PBR^{-1}B'P + Q, \ t \neq t_i$$
$$P(\tau_i^-) = A_d(\tau_i)'P(\tau_i^+)A_d(\tau_i) + Q_i, \ t = t_i$$

with $R, Q, Q_i > 0$. The feedback control is given by:

$$u(\tau, x_\perp) = -R^{-1}B(\tau)'P(\tau)x_\perp.$$

Note that there is no nominal control command, since we are stabilizing a passive walking cycle.

To enable the use of SoS optimization, we approximate the non-polynomial dynamics of the walker via a third order

Taylor expansion. This expansion is performed around each of the N sample points.

The Riccati equation provides us with an initial candidate Lyapunov function:

$$V_0(x_\perp, \tau) = \sigma_0 x'_\perp P(\tau) x_\perp.$$

Taking a suitably small σ_0, we find a valid region of attraction. To optimize the region of attraction, we rescale V_0 by a polynomial $\rho : [0, T] \mapsto (0, \infty)$:

$$V(x_\perp, \tau) = \frac{1}{\rho(\tau)} V_0(x_\perp, \tau).$$

We maximize the integral of $\rho(t)$ over the interval as a surrogate for the volume of the region of attraction. For the compass gait system this parameterization proved better numerically conditioned than directly scaling the Lyapunov function. The following observations allow our constraints to remain linear in the parameters of $\rho(t)$. Note that:

$$\frac{d}{dt} V(x_\perp, \tau) = \frac{1}{\rho(\tau)^2} \left[\rho(\tau) \frac{d}{dt} V_0(x_\perp, \tau) - \frac{\partial \rho}{\partial \tau} \dot{\tau} V_0(x_\perp, \tau) \right],$$

To enforce $\frac{d}{dt} V(x_\perp, \tau) \leq -\delta |x_\perp|^2$, we can exploit the fact that δ can be an arbitrary positive constant, and instead require:

$$\rho(\tau) \frac{d}{dt} V_0(x_\perp, \tau) - \frac{\partial}{\partial \tau} \rho(\tau) \dot{\tau} V_0(x_\perp, \tau) \leq \delta_0 |x_\perp|^2.$$

As $\rho(t)$ is bounded above on $[0, T]$ an appropriate δ exists. Finally, $\{x \mid V(x_\perp, \tau) < 1\}$ is identically $\{x \mid V_0(x_\perp, \tau) < \rho(\tau)\}$. Figure 12 presents overlapped plots of the region of attraction projected into the $(\theta_1, \dot{\theta}_1)$ and $(\theta_2, \dot{\theta}_2)$ planes.

These regions indicate that the controller can stabilize much larger variations in the swing-leg than in the stance-leg, which matches intuition on the compass gait walker.

A. Accuracy of Taylor Expansion

Since we are approximating the dynamics by a Taylor expansion, it is important to check whether we can trust the verification. To examine this approximation, we sample points on the boundary of the certified region of attraction. For each point, we compute $\frac{d}{dt} V(x_\perp, \tau)$ with the true dynamics and Taylor expansion approximation. At each time step we sampled 10,000 points from the boundary. In Figure 13 we plot the true value of $\frac{d}{dt} V$ against the approximation error. Note that the vertical scale of the plot is approximately 10^{-5} vs. an almost unit scaling along the horizontal, and essentially all the points are to the left of zero.

Of the 400,000 samples, 104 had $\frac{d}{dt} V > 0$, so the verification using Taylor series was correct at 99.97% of samples. The largest value of $\frac{d}{dt} V$ was 0.0026. Note that isolated samples of positive $\frac{d}{dt} V$ do not necessarily imply instability from that point, it is possible (indeed, likely) that the Lyapunov function was not appropriate for proving stability at that point.
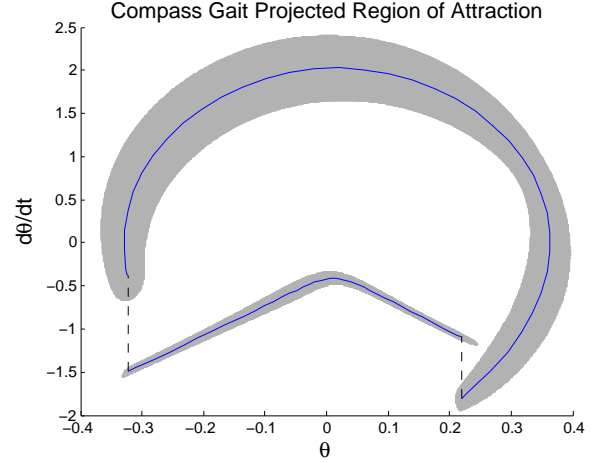

Fig. 12. Regions of Attraction for the compass-gait walker limit cycle. We present two of six possible projections of the RoA. The upper curve plots the trajectory and RoA projected into the $(\theta_1, \dot{\theta}_1)$ plane, that of the "swing leg". The lower curve is the equivalent for the "stance" leg coordinates $(\theta_2, \dot{\theta}_2)$.
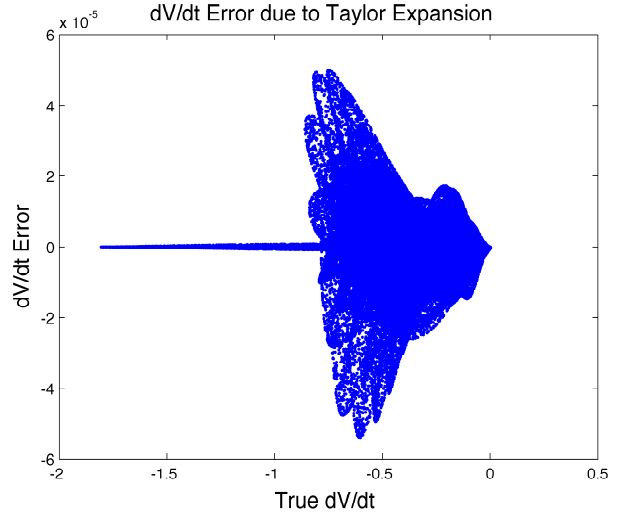

Fig. 13. The above compares the rate of change of the Lyapunov function for the true and Taylor expanded dynamics at the boundary of the approximate region-of-attraction. 99.7% of samples were verified correctly.

B. Computation Times

In computing the regions of attraction, we alternate between optimizing over $V(x_\perp, \tau)$ – a "V-step", and optimizing over Lagrange multipliers – an "L-step". It took four V-L iterations until covergence. The computations were performed on a 2.66 GHz intel Core i7 processor with 8GB of RAM, and timings for each iteration are shown in Table VI-B. The total computation time was around 17.7 minutes.

Note, however, that due to the sampling in τ, each L-step is made up of 41 independent optimizations (40 continuous samples and one impact map) each of which took between 1.6 and 2.6 seconds. Since these computations are trivially

Iteration	1	2	3	4
L-step time (s)	75.0	90.2	80.8	78.7
V-step time (s)	194	183	201	170

TABLE I

COMPUTATION TIMES FOR THE COMPASS-GAIT WALKER.

parallelizable, substantial speed increases could be achieved on multiprocessor machines.

VII. SUMMARY AND FUTURE WORK

The purpose of this paper has been to demonstrate the application of a new method for estimating regions of attraction for nonlinear hybrid limit cycles. Three simple examples were chosen that elucidated important aspects of the technique, including selection of transversal surfaces, the handling of impacts, optimization of the Lyapunov function, and control design.

This work can be extended in a number of directions. It will serve as an essential component in recent algorithms for feedback control and motion planning in [3]. Implementation on more complex models and experimental validation will be an important test.

In this paper we searched for regions via τ-varying rescalings of quadratic Lyapunov functions from linear theory. This was done primarily to simplify the optimization procedure, however in principle it is possible to search over any polynomial Lyapunov functions, which would presumably give substantially bigger (and possibly asymmetric) regions for many systems.

There are many connections between sum-of-squares verification and robust control and stability theory via integral quadratic constraints ([23], [24]) which will be investigated.

REFERENCES

[1] I. R. Manchester, "Transverse dynamics and regions of stability for nonlinear hybrid limit cycles," *under preparation*, 2010.

[2] S. H. Collins, A. Ruina, R. Tedrake, and M. Wisse, "Efficient bipedal robots based on passive-dynamic walkers," *Science*, vol. 307, pp. 1082–1085, February 18 2005.

[3] R. Tedrake, I. R. Manchester, M. M. Tobenkin, and J. W. Roberts, "LQR-Trees: Feedback motion planning via sums of squares verification," *International Journal of Robotics Research*, vol. 29, pp. 1038–1052, July 2010.

[4] R. D. Gregg, T. W. Bretl, and M. W. Spong, "Asymptotically stable gait primitives for planning dynamic bipedal locomotion in three dimensions," in *IEEE International Conference on Robotics and Automation*, Anchorage, AK, 2010, pp. 1695–1702.

[5] J. K. Hale, *Ordinary Differential Equations*. Robert E. Krieger Publishing Company, New York, 1980.

[6] N. Z. Shor, "Class of global minimum bounds of polynomial functions," *Cybernetics and Systems Analysis*, vol. 23, no. 6, pp. 731–734, November 1987.

[7] P. A. Parrilo, "Structured semidefinite programs and semialgebraic geometry methods in robustness and optimization," Ph.D. dissertation, California Institute of Technology, May 18 2000.

[8] ——, "Semidefinite programming relaxations for semialgebraic problems," *Mathematical Programming*, vol. 96, no. 2, pp. 293–320, 2003.

[9] U. Topcu, A. Packard, and P. Seiler, "Local stability analysis using simulations and sum-of-squares programming," *Automatica*, vol. 44, no. 10, pp. 2669 – 2675, 2008.

[10] W. Tan and A. Packard, "Stability region analysis using polynomial and composite polynomial Lyapunov functions and sum-of-squares programming," *IEEE Transactions on Automatic Control*, vol. 53, no. 2, pp. 565–571, March 2008.

[11] D. Henrion and A. Garulli, Eds., *Positive Polynomials in Control*, ser. Lecture Notes in Control and Information Sciences. Springer-Verlag, 2005.

[12] J. M. Goncalves, "Regions of stability for limit cycle oscillations in piecewise linear systems," *IEEE Transactions on Automatic Control*, vol. 50, no. 11, pp. 1877–1882, 2005.

[13] C. S. Hsu, "A theory of cell-to-cell mapping dynamical systems," *Journal of Applied Mechanics*, vol. 47, no. 4, pp. 931–939, 1980.

[14] A. L. Schwab and M. Wisse, "Basin of attraction of the simplest walking model," *Proceedings of the ASME Design Engineering Technical Conference*, vol. 6, pp. 531–539, Sep 2001.

[15] J. Hauser and C. C. Chung, "Converse lyapunov functions for exponentially stable periodic orbits," *Systems & Control Letters*, vol. 23, no. 1, pp. 27 – 34, 1994.

[16] A. S. Shiriaev, L. B. Freidovich, and I. R. Manchester, "Can we make a robot ballerina perform a pirouette? orbital stabilization of periodic motions of underactuated mechanical systems," *Annual Reviews in Control*, vol. 32, no. 2, pp. 200–211, Dec 2008.

[17] M. J. Coleman, "A stability study of a three-dimensional passive-dynamic model of human gait," Ph.D. dissertation, Cornell University, 1998.

[18] A. Goswami, B. Thuilot, and B. Espiau, "A study of the passive gait of a compass-like biped robot: symmetry and chaos," *International Journal of Robotics Research*, vol. 17, no. 12, 1998.

[19] M. W. Spong and F. Bullo, "Controlled symmetries and passive walking," *IEEE Transactions on Automatic Control*, vol. 50, no. 7, pp. 1025–1030, Jul 2005.

[20] E. R. Westervelt, J. W. Grizzle, C. Chevallereau, J. H. Choi, and B. Morris, *Feedback Control of Dynamic Bipedal Robot Locomotion*. CRC Press, Boca Raton, FL, 2007.

[21] K. Byl and R. Tedrake, "Metastable walking machines," *International Journal of Robotics Research*, vol. 28, no. 8, pp. 1040–1064, August 1 2009.

[22] I. R. Manchester, U. Mettin, F. Iida, and R. Tedrake, "Stable dynamic walking over rough terrain: Theory and experiment," in *Proceedings of the International Symposium on Robotics Research (ISRR)*, 2009.

[23] A. Megretski and A. Rantzer, "System analysis via integral quadratic constraints," *IEEE Transactions on Automatic Control*, vol. 42, no. 6, pp. 819 –830, Jun 1997.

[24] I. R. Petersen, V. A. Ugrinovskii, and A. V. Savkin, *Robust Control Design using H^∞ Methods*. Springer-Verlag, 2000.